Southern Ocean frontal structure and sea-ice formation rates revealed by elephant seals

J.-B. Charrassin[a,b], M. Hindell[c], S. R. Rintoul[d], F. Roquet[a], S. Sokolov[d], M. Biuw[e], D. Costa[f], L. Boehme[g], P. Lovell[g], R. Coleman[h], R. Timmermann[i], A. Meijers[h], M. Meredith[j], Y.-H. Park[a], F. Bailleul[k], M. Goebel[l], Y. Tremblay[f], C.-A. Bost[k], C. R. McMahon[m], I. C. Field[m], M. A. Fedak[g], and C. Guinet[k]

[a]Unité Scientifique du Muséum 402/Laboratoire d'Océanographie et du Climat: Expérimentation et Approches Numériques, Département Milieux et Peuplements Aquatiques, Muséum National d'Histoire Naturelle, 43 rue Cuvier, 75231 Paris Cedex 05, France; [c]Antarctic Wildlife Research Unit, School of Zoology, University of Tasmania, P.O. Box 252-05, Hobart TAS 7001, Australia; [d]Wealth from Oceans National Research Flagship and Antarctic Climate and Ecosystems Cooperative Research Centre, Commonwealth Scientific and Industrial Research Organization, Hobart TAS 7001, Australia; [g]NERC Sea Mammal Research Unit, Gatty Marine Laboratory, University of St. Andrews, St. Andrews, Fife KY16 8LB, United Kingdom; [f]Center for Ocean Health, Institute of Marine Sciences, Long Marine Laboratory, University of California, 100 Shaffer Road, Santa Cruz, CA 95060; [h]Center for Marine Science, University of Tasmania, Private Bag 78, Hobart, TAS 7001, Australia; [i]Alfred Wegener Institute for Polar and Marine Research, Bremerhaven, Germany; [j]British Antarctic Survey, High Cross, Madingley Road, Cambridge CB3 0ET, United Kingdom; [k]Centre d'Etudes Biologiques de Chizé, Centre National de la Recherche Scientifique, Villiers-en-Bois, F-79360 Beauvoir sur Niort, France; [l]Antarctic Ecosystem Research Division, NOAA/National Marine Fisheries Service, 8604 La Jolla Shores Drive, La Jolla, CA 92037-1508; [m]School for Environmental Research, Charles Darwin University, Darwin NT 0909, Australia; and [e]Norwegian Polar Institute, Polar Environmental Centre, NO-9296 Tromsø, Norway

Edited by Hugh Ducklow, Marine Biological Laboratory, Woods Hole, MA, and accepted by the Editorial Board June 3, 2008 (received for review January 25, 2008)

Polar regions are particularly sensitive to climate change, with the potential for significant feedbacks between ocean circulation, sea ice, and the ocean carbon cycle. However, the difficulty in obtaining *in situ* data means that our ability to detect and interpret change is very limited, especially in the Southern Ocean, where the ocean beneath the sea ice remains almost entirely unobserved and the rate of sea-ice formation is poorly known. Here, we show that southern elephant seals (*Mirounga leonina*) equipped with oceanographic sensors can measure ocean structure and water mass changes in regions and seasons rarely observed with traditional oceanographic platforms. In particular, seals provided a 30-fold increase in hydrographic profiles from the sea-ice zone, allowing the major fronts to be mapped south of 60°S and sea-ice formation rates to be inferred from changes in upper ocean salinity. Sea-ice production rates peaked in early winter (April–May) during the rapid northward expansion of the pack ice and declined by a factor of 2 to 3 between May and August, in agreement with a three-dimensional coupled ocean–sea-ice model. By measuring the high-latitude ocean during winter, elephant seals fill a "blind spot" in our sampling coverage, enabling the establishment of a truly global ocean-observing system.

Antarctic Circumpolar Current | instrumentation | marine predators | ocean observation | sea-ice modeling

Evidence that the polar oceans are changing is growing rapidly, particularly in the northern hemisphere, where a significant decline in sea ice (1) and changes in the freshwater budget have been observed (1, 2). In the southern hemisphere, the limited observations available suggest that the circumpolar Southern Ocean has warmed more rapidly than the global ocean average (3) and that the dense water formed near Antarctica and exported to lower latitudes has freshened in some locations (4, 5) and warmed in others (6, 7). However, studies of change in the polar oceans as well as investigations of high-latitude dynamics continue to be hampered by a paucity of observations. In particular, although satellites and profiling floats are now providing measurements of much of the global ocean (8), the ocean beneath the Antarctic sea ice remains almost entirely unobserved. At ≈19 million km^2 at maximum extent (9), this represents a vast area. Sea-ice cover prohibits remote sensing of the underlying ocean by satellites, prevents conventional Argo floats from surfacing to transmit data, and makes ship operations expensive, difficult, and slow. Efforts are currently underway to develop ice-capable autonomous floats (10), but existing observations are heavily biased toward summer and open water.

Observations of sea ice itself are also sparse, particularly in the Antarctic. Whereas the surface characteristics of sea ice can be measured by satellite, the key climate parameters sea-ice thickness and formation rate cannot be observed by using remote sensing. The formation rate determines how much brine is released and therefore the potential to form high-salinity shelf water, the precursor to Antarctic Bottom Water. Sea-ice net growth rate is therefore an essential parameter to validate in climate models. Existing estimates of Antarctic sea-ice production, however, are limited to two special and extreme cases: landfast ice, where the continuous ice surface minimizes air–sea heat exchange and therefore ice production (11), and coastal polynyas, where the absence of ice results in intense air–sea exchange and very high ice production and export (12). No measurements have been made of ice production in the mobile pack of mixed ice types and ages typical of the vast majority of the Antarctic continental shelf.

Southern elephant seals (*Mirounga leonina*) regularly spend the winter feeding within the sea-ice pack and high-latitude waters of the Southern Ocean. To study the foraging ecology of elephant seals in relation to oceanographic conditions, 58 animals were equipped with high-accuracy conductivity–temperature–depth satellite-relayed data loggers (CTD-SRDLs) during 2004–2005 at four sub-Antarctic islands (13, 14). Here, we show that measurements collected by these long-ranging, deep-diving predators allow the high-latitude fronts of the Southern Ocean to be mapped in regions and at times of year not sampled by other oceanographic instruments, and allow sea-ice-formation rates to be inferred from changes in salinity.

Results and Discussion

The elephant seal tracks provided geographic coverage highly complementary to conventional sampling during the same period (Fig. 1). Fig. 1*A* shows the distribution of hydrographic

Author contributions: J.-B.C., M.H., S.R.R., F.R., M.B., D.C., L.B., R.C., M.M., Y.-H.P., C.-A.B., M.A.F., and C.G. designed research; J.-B.C., M.H., M.B., F.B., M.G., Y.T., C.R.M., I.C.F., M.A.F., and C.G. performed research; P.L. and M.A.F. developed hardware and analytical tools; J.-B.C., S.R.R., F.R., S.S., L.B., R.C., R.T., and A.M. analyzed data; and J.-B.C., M.H., S.R.R., and R.C. wrote the paper.

The authors declare no conflict of interest.

This article is a PNAS Direct Submission. H.D. is a guest editor invited by the Editorial Board.

Freely available online through the PNAS open access option.

[b]To whom correspondence should be addressed. E-mail: jbc@mnhn.fr.

This article contains supporting information online at www.pnas.org/cgi/content/full/0800790105/DCSupplemental.

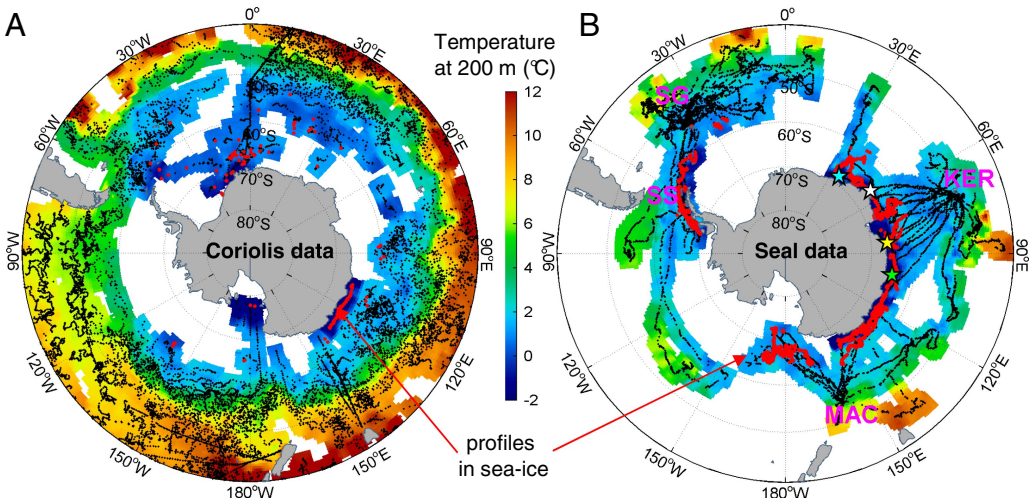

Fig. 1. Circumpolar distribution of hydrographic profiles and temperature at 200 m from the Coriolis database and data collected by elephant seals in the Southern Ocean during 2004–2005. (*A*) Data from the Coriolis database consisting in Argo floats, XBTs, and research vessels. (*B*) Data collected by elephant seals equipped with CTD-SRDLs at South Georgia (SG), and South Shetland (SS), Kerguelen, (KER), and Macquarie (MAC) islands. Red points indicate profiles collected in sea ice. Color stars indicate positions of time series collected in sea ice by four different seals (see Table 1).

profiles (n = 14,470) collected during 2004–2005 by Argo floats, ships, and expendable bathythermographs (XBTs) (Coriolis data). Profiles from these sources are abundant between 40°S and 60°S, but the number decreases dramatically south of 60°S, with only 148 profiles acquired within the sea-ice zone. Accordingly, the map of ocean temperature at 200 m produced from these measurements is almost complete north of 60°S but shows large gaps farther south (Fig. 1*A*). While exploring their high-latitude feeding grounds in autumn and winter, seals covered areas not sampled by conventional techniques in the Southern Indian Ocean and along the margin of East Antarctica, near the Antarctic Peninsula, and north of the Ross Sea (Fig. 1*B*). Seals from Kerguelen and Macquarie Islands headed south and foraged along east Antarctica and the ice-edge north of the Ross Sea during autumn and winter. South Georgia seals explored oceanic waters in the Scotia Sea, and those from South Shetlands ventured into the southeast Pacific, while both groups also foraged along the western side of the Antarctic Peninsula (Fig. 1*B*) (the foraging ecology of different seal populations is discussed in ref. 14). Seals dove repeatedly, transmitting 2.1 ± 0.8 temperature (T) and salinity (S) profiles per day on average, to a mean depth of 566 ± 89 m and a maximum depth of 1,998 m [supporting information (SI) Table S1]. The seals typically covered distances of 35–65 km per day, resulting in a spatial resolution along the foraging track of ≈25 km, compared with a typical spacing of 50 km or more for a high-resolution hydrographic section obtained by a research vessel (Table S1). A total of 16,500 seal profiles were acquired (Fig. 1*B*), including 8,200

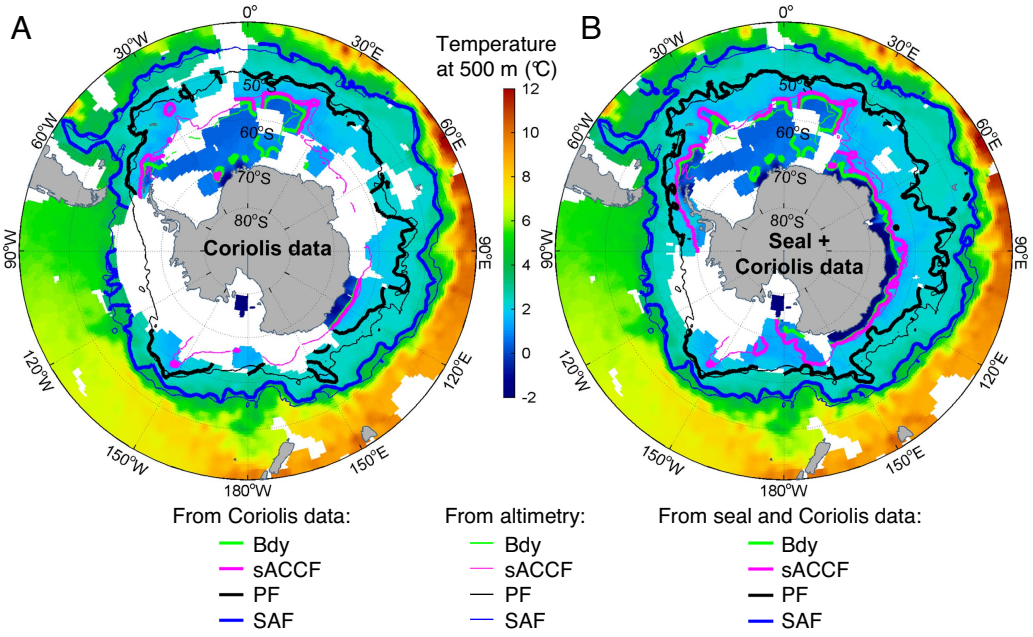

Fig. 2. Temperature field at 500 m during 2004–2005 from the Coriolis database and from the merged Coriolis and elephant seal databases. Mean front positions during the same period derived from Coriolis (*A*) or Coriolis and seal temperature field at 500 m (*B*) (thick lines), and from altimetry (thin lines in *A* and *B*). Plotted fronts are Bdy, southern branch of sACCf, and central branches of PF and SAF. Note the increased level of detail in the combined plots.

profiles south of 60°S, i.e., nine times more than obtained from floats and ships. The temperature fields agree in regions covered by both data sources (e.g., the Scotia Sea and sub-Antarctic Indian Ocean; Fig. 1). The 4,520 seal profiles from within the sea ice represent a 30-fold increase over conventional data, with 90% of profiles acquired during austral autumn and winter when conventional observations are scarce (in 2004–2005, only 148 autumn–winter profiles in the sea-ice zone were obtained from ships and floats).

By combining observations from seals, floats, and ships, we mapped water properties throughout most of the Southern Ocean, including under the winter sea ice. In particular, the seal profiles allowed the position of the major high latitude fronts of the Southern Ocean to be determined with greater spatial coverage and accuracy than is possible using only ship and float profiles. The Antarctic Circumpolar Current (ACC) consists of three main fronts, from north to south: the Subantarctic Front (SAF), the Polar Front (PF), and the southern ACC front (sACCf). The southern boundary of the ACC (Bdy), which corresponds to the southernmost edge of the Upper Circumpolar Deep Water signal, marks the southern limit of the circumpolar flow (15). Knowledge of the frontal locations is important because eddies spawned from instabilities of the fronts play a crucial role in the dynamical and thermodynamical balance of the Southern Ocean (16). The fronts also influence the distribution and magnitude of biological production in the Southern Ocean at all trophic levels from phytoplankton to whales (17, 18). Maps of Southern Ocean fronts have traditionally been constructed from sparse ship observations, with a strong bias to summer (15). Sokolov and Rintoul (19) have shown that the multiple fronts of the ACC can be mapped with improved spatial and temporal resolution using satellite altimetry. However, this method cannot locate fronts beneath sea ice (Fig. 2). At the time of maximum ice extent (September–October), only 15% (49%) of the near-circumpolar path of the Bdy (southern branch of the sACCf) can be mapped using altimetry. Even in summer (minimum ice extent), only 15% and 63% of the Bdy and southern branch of the sACCf, respectively, can be mapped by using altimetry (Fig. 2).

Here, we use the seal data to extend the frontal maps to ice-covered areas by exploiting a tight relationship between sea-surface height and temperature at 500 m depth (see *Materials and Methods* and Fig. S1). Using ship and float profiles alone, the sACCf and Bdy can be identified in only a few regions (Fig. 2*A*). When the seal profiles are added, almost the entire circumpolar extent of each of the fronts can be mapped, with the exception of the southeast Pacific (the lack of islands in the Pacific sector suitable for elephant seal breeding contributes to the gap there) (Fig. 2*B*). The fraction of the circumpolar distribution of the southernmost ACC fronts that can be mapped increases from 25% to 68%, 27% to 74%, and 49% to 85% for the Bdy, southern, and northern branches of the sACCf, respectively, when the combined dataset is used (Fig. 2*B*). The largest increases are located in the Southern Indian Ocean, north of the Ross Sea, and the Western Antarctic Peninsula. The path of the southern fronts of the ACC can thus only be determined when the seal data are used to complement the sampling by ships, floats, and satellites. Furthermore, the spatial resolution of the frontal maps derived from the combined data set is much greater than those obtained from traditional hydrographic climatologies (15) (Fig. S2).

Formation of sea ice releases brine and drives the production of dense waters that form the lower limb of the global thermohaline circulation. However, the rate of sea-ice formation remains poorly known because sea-ice production cannot be measured remotely, and *in situ* observations in winter sea ice are scarce. Seal measurements of changes in salinity below the sea ice provide a unique dataset with which to constrain estimates of

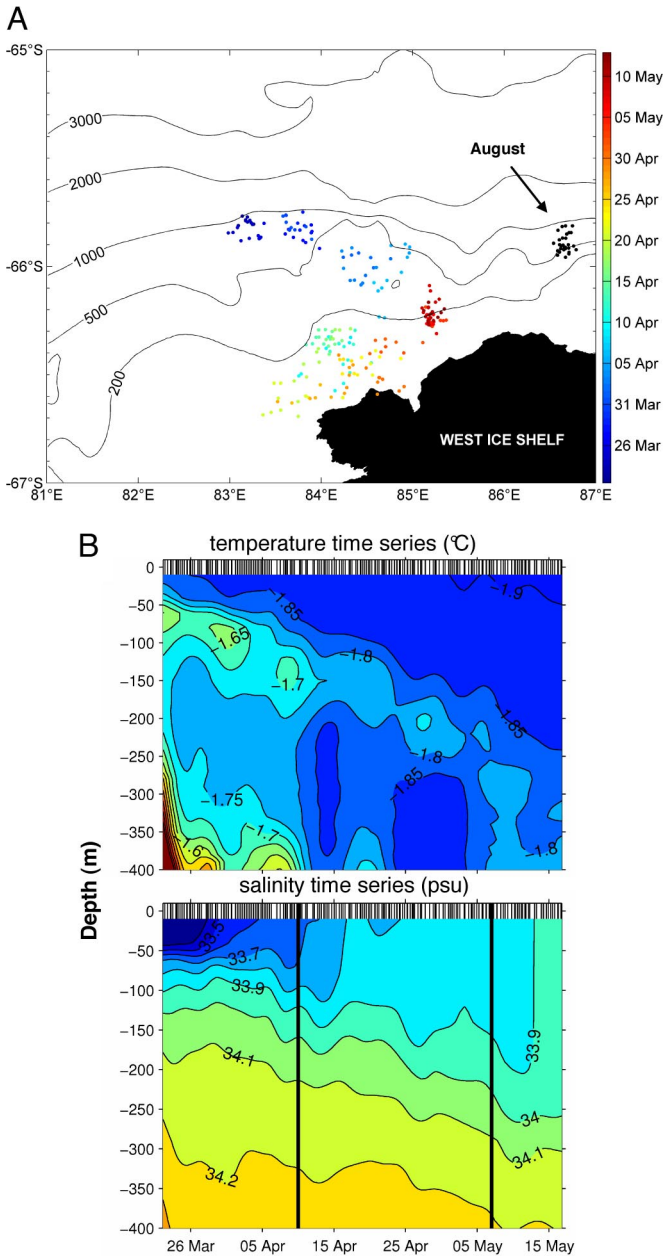

Fig. 3. Time series of hydrological properties collected by an elephant seal in sea ice over the continental shelf. (*A*) Positions of CTD profiles collected by a seal near 84°E in April–May 2004 (color dots), and in August 2004 (black dots). The outline of the West Ice Shelf was obtained from Moderate Resolution Imaging Spectroradiometer (MODIS) data. (*B*) T and S measured by this seal in April–May 2004 near 84°E (indicated by a yellow star on Fig. 1*B*); for T and S time series, small vertical bars indicate profiles collection; the large vertical bars on S time series delimit the period over which the sea-ice formation rate was estimated.

net sea-ice formation. Fig. 3 shows a time series of temperature and salinity from a seal that collected 200 profiles over 50 days on the continental shelf at 84°E, and which exemplifies the data that the seals in ice provided. The seal entered the sea ice on 22 March and crossed the shelf break and the Antarctic Slope Front on 10 April, as indicated in Fig. 3*B* by the transition to colder temperatures and deeper isohalines. The seal then remained in a small area ($\approx 80 \times 30$ km^2) on the continental shelf near the West Ice Shelf for the next 28 days (Fig. 3*A*). Shelf water temperatures were close to the surface freezing point, and the

Table 1. Sea-ice formation rates estimated from changes in salinity measured by elephant seals in 2004

Seal	Position	No. of profiles	Mean sea-ice concentration, % (AMSR-E data)	Mean sea-ice formation rate, cm·d^{-1}	Thickness of sea ice formed, m	Averaging period
1	34°E, 68.2°S	90	85 ± 16	2.7	0.68	9 April to 3 May
2	54°E, 65.4°S	82	75 ± 20	3.0	0.76	4–28 April
3	84°E, 66.5°S	84	80 ± 24	2.4	0.68	10 April to 7 May
3	84°E, 66.5°S	119	86 ± 15*	1.08	1.12	7 May to 17 August
4	103°E, 65.2°S	177	64 ± 27	0.8	0.40	15 May to 4 July

AMSR-E, Advanced Microwave Scanning Radiometer–Earth Observing System.
*Mean sea-ice concentration was calculated over 10–17 August.

sea-ice concentration was 80 ± 24%. Brine released during sea-ice formation caused a rapid increase in the salinity (by 0.17) and depth (from 65 to 175 m) of the surface mixed layer. Assuming that the salinity increase is driven by local sea-ice production (20), formation of 0.68 m of sea ice over 28 days (2.4 cm·d^{-1}) is required to explain the change in salinity in the upper 100 m of the water column (see *Materials and Methods*). The same seal returned to the area 3 months later, in August (Fig. 3*A*). The mixed layer depth had increased to 220 m, the temperature was at the surface freezing point throughout the upper 400 m, and the salinity of the upper 100 m had increased by a further 0.24 (Fig. S3) corresponding to formation of an additional 1.12 m of sea ice between May and August at an average rate of 1.1 cm·d^{-1}. Three other seals remained in one location for periods of 3 to 7 weeks, allowing sea-ice formation rates to be estimated at four locations between 34°E and 103°E (Table 1 and Figs. S4–S6). A similar time history is observed at each site: the maximum sea-ice formation rates are observed in late April to early May (range of 2.4–3.0 cm·d^{-1}); lower values of 0.8–1.1 cm·d^{-1} are found for the period mid-May to July–August.

Previous estimates of sea-ice formation rates have been restricted to two limiting cases, coastal polynyas and landfast ice. In coastal polynyas, where intense ocean heat loss drives rapid ice production, estimates of ice formation rates vary from 10 cm·d^{-1} [average rate over 90 days in winter, calculated from air–sea heat flux (21)] to 8 cm·d^{-1} from ice thickness change measured along the trajectory of drifting buoys over a 3-week period in August 1999 (22) and 5.8 cm·d^{-1} from salt budget calculations for the same experiment (23). At the other extreme, landfast ice tends to inhibit heat loss by the ocean and reduce ice formation rates. The time history of fast ice thickness near 63°E in 1969 reported in ref. 11 implies an ice formation rate of 2.2 cm·d^{-1} between 10 April and 5 May and a rate of 0.6 cm·d^{-1} between May and 27 August. Our estimates for the consolidated pack ice (mean concentration of ≈80%; Table 1) typical of most of the Antarctic continental shelf fall between estimates from these two extreme cases of air–sea interaction.

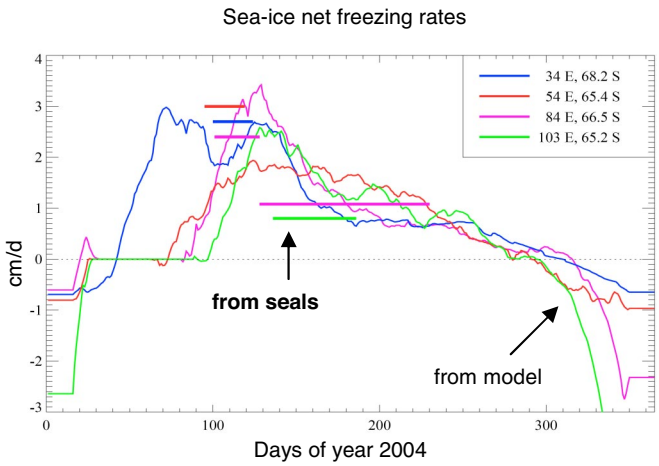

Fig. 4. Sea-ice net freezing rates derived from the seal data and from a coupled sea ice–ocean model (FESOM) (24). Thin lines indicate daily net freezing rates from the model, extracted at four grid points closest to the respective seal positions (Fig. S7) and smoothed with a 31-d running mean. Thick horizontal line segments correspond to sea-ice formation rates inferred from the salinity budgets measured by seal 1, 2, 3, and 4 at 34°E, 54°E, 84°E, and 103°E, respectively (Table 1). Length of segment indicates the averaging interval.

Our inference of a rapid increase to a maximum in late April to early May, followed by slower ice formation as the pack consolidates and inhibits air–sea heat exchange, agrees well in timing and magnitude with results of a coupled sea ice–ocean model (Fig. 4 and Figs. S7 and S8) (24). Sea ice in the model begins to form in March or April, reaches a peak in late April or early May, and declines to net formation rates close to zero in August. The maximum of observed net freezing rates (seal data) is found at a position very close to the coast at 54°E, where the model's resolution appears to be too coarse to capture the peak freezing rates. For the locations at 34°E, 84°E, and 103°E, we find a good agreement between modeled and observed data.

The global thermohaline circulation and climate system are sensitive to changes in the freshwater balance at high latitudes (25). Year-round, sustained, broad-scale measurements of ocean temperature and salinity are needed to detect and explain changes in the freshwater budget in the polar and subpolar oceans. Our ability to represent the high-latitude oceans and sea ice in oceanographic and climate models also suffers from the lack of observations for model testing, data assimilation, and improved process understanding. Conventional oceanographic platforms cannot provide such observations under the sea ice, particularly on the Antarctic continental shelf, where the most important water mass transformations take place. Seals equipped with oceanographic sensors can help fill this gap by measuring water properties over broad areas in winter, when few other measurements are available. Here, we have demonstrated that by combining traditional oceanographic data and seal observations, the circumpolar path of the southern fronts of the ACC can be resolved in great detail. Furthermore, the seals provide the first time series of upper ocean salinity changes in winter over the Antarctic continental shelf, from which sea-ice formation rates can be inferred. The oceanographic information obtained is a valuable by-product of the use of tags to develop insights into the influence of the physical environment on the foraging ecology of seals. An expanded array of polar marine predators equipped with environmental sensors, including seal species that target different foraging areas, would provide a powerful and cost-effective means to make the ocean-observing system truly global.

Materials and Methods

Instrumentation. CTD–Satellite Relay Data Loggers (CTD-SRDLs) were built by the Sea Mammal Research Unit (SMRU) (University of St. Andrews, Scotland), incorporating CTD sensors developed by Valeport. The sensor head consists of a pressure (P) transducer, a platinum resistance thermometer, and an induc-

tive cell for measuring conductivity. Whenever possible, a thorough calibration and testing procedure should be undertaken for any new device, which should include predeployment laboratory calibrations of the tags, an at-sea validating test immediately before deployment, and, importantly, comparison of postdeployment data with all available concurrent and historical data. This procedure was followed for most deployments in this study. Before being taken into the field, devices were calibrated at Valeport, Service Hydrographique de la Marine (Brest, France), or Naval Postgraduate School (Monterey, CA), and had temperature (T) and conductivity (C) resolutions of 0.001°C and 0.002 mS/cm, respectively. Instruments deployed at Kerguelen (2004–2005) and at South Georgia (2005) were checked at sea against conventional CTDs and validated. Data were further corrected by using the closest available historical deep salinity (S) measurements (>400 m) [Kerguelen data (26)] or the closest contemporaneous Argo and ship data (South Georgia and Macquarie T and S data; method modified from ref. 27). Overall, corrected P, T, and S had accuracies of 2 dbar, 0.02–0.03°C, and 0.03–0.05 practical salinity units (psu), respectively. The T and S seal profiles provide a detailed hydrographic picture of the upper ocean (Fig. S9 *A–C*)as illustrated by the strong consistency between concurrent SSHs derived from seal data and from combined altimetry/climatology along a cross-ACC section (Fig. S9*D*). The accuracy of CTD-SRDL sensors has been continuously improved since 2005.

Deployment on Seals. Instruments were deployed on southern elephant seals at the end of their molt in late summer to cover their prebreeding, winter foraging trips. Animals were anesthetized with i.v. tiletamine and zolazepam 1:1 (28), and then instruments were attached to the fur on their head by using a two-component industrial epoxy. Seals dove repeatedly with CTD data being collected every 4 s during the ascent phase of dive and processed onboard before being transmitted via the Argos satellite system when animals were at the surface (13, 14). On average, 2.1 ± 0.8 vertical temperature (T) and conductivity (C) profiles were transmitted daily. Because of the narrow bandwidth of Argos transmitters, each profile was transmitted in a compressed form consisting of 12 T and C data points corresponding to the most important inflection points determined onboard by using a ''broken stick algorithm'' (29).

Hydrographic Data. Conventional hydrographic data were extracted from the Coriolis database (www.coriolis.eu.org) for the period covered by seal data (27 January 2004 to 22 November 2005). Coriolis is a Global Data Centre (GDAC), a part of the Global Ocean Data Assimilation Experiment (GODAE), and stores hydrographic data available from all sources including Argo Float, XBTs, and ship-based CTDs. Only profiles flagged as ''good data only'' were extracted and included two processing levels (real-time and delayed mode). They consisted of 89.6% Argo profiles, 10% ship-based TDs or CTDs, and 0.4% XBTs.

Sea-Ice Data. Daily remote-sensing sea-ice-concentration maps, retrieved from the Advanced Microwave Scanning Radiometer–Earth Observing System (AMSR-E), were obtained from the Institut für Umweltphysik Universität Bremen web site (http://iup.physik.uni-bremen.de:8084/amsr/amsre.html). Sea-ice concentrations were available on a 6.25-km-resolution grid. For each seal profile, we extracted the closest sea-ice concentration available for the day of collection in a 8 × 8 km cell centered on the profile, resulting in a mean distance between profiles and sea-ice concentration data point of 2.34 ± 0.87 km (range 0.06–4.31 km). Sea-ice concentrations encountered by seals averaged 79 ± 28% versus 69 ± 33% for conventional platforms.

Mapping of Coriolis and Seal-Derived Sea-Water Temperature. For both Coriolis and seal data, horizontal mapping of sea water temperature data were conducted by using a semioptimal objective mapping procedure. Temperatures at 200 and 500 m were extracted from each transmitted profile by using a linear interpolation between inflection points. Data were then mapped on a global 0.5° × 0.5° grid by using objective analysis with an exponentially decaying covariance function set at a decorrelation length scale of 200 km. To quantify seasonal trends in temperatures at 200 and 500 m collected from January to November, residuals of the objective analysis were plotted against time, and no significant trends were detected for either seal or Coriolis data ($r^2 < 0.01$, $P < 0.001$ for order 3 polynomials).

Front Definition from Altimetry. The major ACC fronts (Bdy, sACCf, PF, and SAF) were identified by using absolute sea surface height (SSH) after ref. 19. Each of the major fronts of the ACC consists of multiple branches, each of which corresponds to a particular value of absolute SSH (i.e., a streamline). Absolute SSH values were calculated by adding the mean SSH anomalies over the study period (January 2004 to November 2005) to the mean surface dynamic height (relative to 2,500 dbar) derived from the World Ocean Circulation Experiment (WOCE) climatology (19, 30). The SSH anomalies are from the CLS/AVISO ''Mean Sea Level Anomaly'' (MSLA) product, produced by mapping data from the Topex/POSEIDON, ERS-1, and ERS-2 satellite altimeters. The SSH value corresponding to each front was determined by fitting absolute SSH contours to 638 weekly maps of gradients of absolute SSH (see ref. 19 for details).

Front Definition from Temperature Fields Constructed from Coriolis and Seal Data. Temperature and salinity profiles from Argo floats were used to determine the relationship between SSH and temperature at 500 m depth (T_{500}) (Fig. S1). The relationship was used to determine the T_{500} value corresponding to the SSH value applicable to each front (19). The Bdy, southern sACCf, central PF, and central SAF branches were found to coincide with T_{500} = 0.82°C, 1.28°C, 2.20°C, and 3.58°C, respectively. The mean spatial error in mapping the fronts by using this relationship was estimated to 31 ± 18 km (see Fig. S1). The front definitions based on these T_{500} values agree well with traditional front definition criteria that account for multiple branches of the fronts (ref. 15 as modified in refs. 19 and 31) as shown in Fig. S9*D*. When comparing with ref. 15 only (Fig. S2), we found a general good agreement; discrepancies between the maps such as those observed for the PF in the Indian Sector of the SO largely reflect the multiple branches of the ACC fronts (not taken into account in ref. 15), larger spatial smoothing in the climatological map, and the different time periods covered in the two cases.

Estimation of Sea-Ice Formation Rate. The rate of sea-ice formation is inferred from a salt budget for the upper 100 m of the water column: $\rho_o V_o S_o = \rho_o V_f S_f + \rho_i V_i S_i$, where ρ_o is the sea water density = 1,027 kg·m^{-3}; V_o is the initial volume of water, with salinity S_o; V_i is the volume of ice formed with density ρ_i = 920 kg·m^{-3} and salinity S_i = 10 (32); and $V_f = V_o - V_i$ is the final volume of sea water with salinity S_f. By considering the time series recorded by individual seals, we focus on relative changes over time and do not need to rely on the accuracy of the absolute salinity calibration of a number of seal sensors. To the extent that salinity increases at depths greater than 100 m are due to brine release, these estimates are lower bounds on the formation rate. The ice formation calculations assume no contribution from horizontal advection (as in ref. 20), which cannot be assessed from the seal data, from entrainment from below, or from precipitation and evaporation. Simulations with a finite-element coupled sea ice–ocean model (see below) indicate that the error caused by these assumptions is typically <0.3 cm/d. The freshening by net precipitation yields the biggest error contribution, suggesting that our calculation tends to underestimate the real sea-ice formation rate.

Sea-Ice Model. Simulated sea-ice formation rates have been derived from a modified version of the Finite-Element Sea Ice–Ocean Model (FESOM) (24). The model consists of a free-surface, hydrostatic primitive-equation ocean model [Finite Element Ocean Model (33)] and a newly implemented dynamic–thermodynamic sea-ice model using an elastic–viscous–plastic rheology. It features a prognostic snow layer and accounts for the effect of snow–ice conversion. Data for this study have been extracted from a circumpolar configuration with 1.5° × 1.5° cos(latitude) horizontal resolution. An open boundary is applied at 48°S, far away from our region of interest. Hydrographic data from World Ocean Atlas 2001 are used for initialization; atmospheric forcing is derived from National Centers for Environmental Prediction/National Center for Atmospheric Research (NCEP/NCAR) reanalysis data. The model simulates regional ocean circulation and seasonal sea-ice coverage in good agreement with observations (Fig. S8).

ACKNOWLEDGMENTS. We thank M. Le Menn (Service Hydrographique de la Marine, Brest) for help with laboratory CTD tags calibration; D. Taillez, B. Olivier, N. Metzl, and S. Blain for at-sea tag calibration; and C. Coatanoan for help with Coriolis data. This work was carried out under the international SEaOS (Southern Elephant seals as Oceanographic Samplers) program (http://biology.st-andrews.ac.uk/seaos). Funding for instrument development was provided by the National Oceanographic Partnership Program–Office of Naval Research (NOPP-ONR). The Sea Mammal Research Unit telemetry team helped develop hardware and analytical tools. The French component was funded by Terre-Océan-Surface Continentale-Atmosphère–Centre National d'Etudes Spatiales (TOSCA-CNES), the Premier Groupe de Mission Mercator Coriolis, and the Institut Polaire Français Paul Emile Victor (IPEV). Support for the Australian component was provided by the Australian Research Council (ARC), the Australian Antarctic Science Grants Scheme (AAS), the Australian Greenhouse Office, the CSIRO Wealth from Oceans National Research Flagship, and the Cooperative Research Centre program of the Australian Government. The United Kingdom component was supported by the Natural Environment Research Council (NERC), and the United States work was funded by the National Science Foundation, National Oceanographic Partnership Program–Office of Naval Research (NOPP-ONR), and the National Undersea Research Pro-

gram–National Oceanic and Atmospheric Administration (NURP-NOAA). Data from Kerguelen seals are available on demand by writing to the Coriolis data service (www.coriolis.eu.org). Data from South Georgia seals are currently available online at the SEaOS web site (http://biology.st-andrews.ac.uk/seaos/results_oceano.htm), and all data will be made available at the SEaOS web site in the near future.

1. Serreze MC, Holland MM, Stroeve J (2007) Perspectives on the Arctic's shrinking sea-ice cover. *Science* 315:1533–1536.
2. Curry R, Mauritzen C (2005) Dilution of the northern North Atlantic Ocean in recent decades. *Science* 308:1772–1774.
3. Gille ST (2002) Warming of the Southern Ocean since the 1950s. *Science* 295:1275–1277.
4. Aoki S, Rintoul SR, Ushio S, Watanabe S, Bindoff NL (2005) Freshening of the Adélie and Bottom Water near 140°E. *Geophys Res Lett* 32:L23601.
5. Rintoul SR (2007) Rapid freshening of Antarctic bottom water formed in the Indian and Pacific oceans. *Geophys Res Lett* 34:L06606.
6. Fahrbach E, Hoppema M, Rohardt G, Schroder M, Wisotzki A (2004) Decadal-scale variations of water mass properties in the deep Weddell Sea. *Ocean Dyn* 54:77–91.
7. Zenk W, Morozov E (2007) Decadal warming of the coldest Antarctic Bottom Water flow through the Vema Channel. *Geophys Res Lett* 34:L14607.
8. Gould WJ, Turton J (2006) Argo—Sounding the oceans. *Weather* 61:17–21.
9. Gloersen P, *et al.* (1992) *Arctic and Antarctic Sea Ice, 1978–1987: Satellite Passive Microwave Observations and Analysis* (National Aeronautics and Space Administration, Washington, DC), NASA SP511, 319 pp.
10. Klatt O, Boebel O, Fahrbach E (2007) A profiling float's sense of ice. *J Atmos Oceanic Technol* 24:1301–1308.
11. Heil P, Allison I, Lytle VI (1996) Seasonal and interannual variations of the oceanic heat flux under a landfast Antarctic sea ice cover. *J Geophys Res Oceans* 101:25741–25752.
12. Markus T, Kottmeier C, Fahrbach E (1998) in *Antarctic Sea Ice Physical Processes, Interactions and Variability*, Antarctic Research Series, ed Jeffries MO (Am Geophys Union, Washington, DC), Vol 74, pp 273–292.
13. Bailleul F, *et al.* (2007) Successful foraging areas of southern elephant seals from Kerguelen Islands in relation to oceanographic conditions. *Philos Trans R Soc London* 362:2169–2181.
14. Biuw M, *et al.* (2007) Variations in behaviour and condition of a Southern Ocean top predator in relation to in-situ oceanographic conditions. *Proc Natl Acad Sci USA* 104:13705–13710.
15. Orsi AH, Whitworth T, Nowlin WD (1995) On the meridional extent and fronts of the Antarctic Circumpolar Current. *Deep-Sea Res I* 42:641–673.
16. Rintoul SR, Hughes CW, Olbers D (2001) in *Ocean Circulation and Climate: Observing and Modelling the Global Ocean*, eds Siedler G, Church J, Gould J (Academic, San Diego), pp 271–302.
17. Tynan CT (1997) Cetacean distributions and oceanographic features near the Kerguelen Plateau. *Geophys Res Lett* 24:2793–2796.
18. Nicol S, *et al.* (2000) Ocean circulation off east Antarctica affects ecosystem structure and sea-ice extent *Nature* 406:504–507.
19. Sokolov S, Rintoul SR (2007) Multiple jets of the Antarctic Circumpolar Current south of Australia. *J Phys Oceanogr* 37:1394–1412.
20. Martinson DG (1990) Evolution of the southern ocean winter mixed layer and sea ice: Open ocean deepwater formation and ventilation. *J Geophys Res Oceans* 95:11641–11654.
21. Cavalieri DJ, Martin S (1985) in *Oceanology of the Antarctic Continental Shelf*, Antarctic Research Series, ed Jacobs SS (Am Geophys Union, Washington, DC), Vol 43, pp 227–252.
22. Lytle VI, *et al.* (2001) Ice formation in the Mertz Glacier polynya, East Antarctica, during winter. *Ann Glaciol* 33:368–372.
23. Williams G, Bindoff NL (2003) Wintertime oceanography of the Adelie Depression. *Deep-Sea Res II* 50:1373–1392.
24. Timmermann R, Danilov S, Schröter JA (2006) A finite element global coupled sea ice-ocean model. *Geophys Res Abstr* 8:07063.
25. Alley RB, *et al.* (2003) Abrupt climate change. *Science* 299:2005–2010.
26. Roquet F, Park Y-H, Guinet C, Bailleul F, Charrassin J-B, Observations of the Fawn Trough Current over the Kerguelen Plateau from instrumented elephant seals. *J Mar Syst*, in press.
27. Böhme L, Send U (2005) Objective analyses of hydrographic data for referencing profiling float salinities in highly variable environments. *Deep-Sea Res II* 52:651–664.
28. McMahon CR, Burton H, McLean S, Slip D, Bester M (2000) Field immobilisation of southern elephant seals with intravenous tiletamine and zolazepam. *Vet Rec* 146:251–254.
29. Lydersen C, *et al.* (2002) Salinity and temperature structure of a freezing Arctic fjord—Monitored by white whales (Delphinapterus leucas). *Geophys Res Lett* 29:2119.
30. Gouretski VV, Koltermann KP (2004) *WOCE Global Hydrographic Climatology* (Berichte des Bundesamt für Seeschifffahrt und Hydrographie, Germany), Technical Report 35.
31. Sokolov S, Rintoul SR (2002) Structure of Southern Ocean fronts at 140°E. *J Mar Syst* 37:151–184.
32. Martin S, Kauffman P (1981) A field and laboratory study of wave damping by grease ice. *J Glaciol* 27:283–313.
33. Danilov S, Kivman G, Schröter J (2004) A finite element ocean model: Principles and evaluation. *Ocean Model* 6:125–150.